

Surface-consistent amplitude corrections for single or multicomponent sources and receivers using reciprocity and waveform inversion

R. van Vossen,¹ A. Curtis^{2,3} and J. Trampert¹

¹*Department of Earth Sciences, Utrecht University, Budapestlaan 4, 3584 CD Utrecht, the Netherlands. E-mail: vossen@geo.uu.nl*

²*School of GeoSciences, The University of Edinburgh, Grant Institute, West Mains Road, Edinburgh, EH9 3JW, UK*

³*Formerly Schlumberger Cambridge Research, High Cross, Madingley Road, Cambridge CB3 0EL, UK*

Accepted 2006 January 5. Received 2005 October 19; in original form 2004 December 8

SUMMARY

In land seismics, near-surface conditions often vary within surveys, resulting in differences in source strength and signature. Furthermore, discrepancies between closely spaced recordings are also commonly observed. Processing and interpretation of recorded data require that data are corrected for these source and receiver perturbations in the early stages of processing. However, existing surface-consistent deconvolution techniques are applicable to primary reflection data only, and therefore require that ground roll and multiples are suppressed prior to the application. This is usually performed with multichannel filter operations. The performance of these filter operations, however, rapidly deteriorates in presence of acquisition-related amplitude and phase perturbations. We propose an alternative approach to compensate for acquisition-related amplitude perturbations, which has the advantage of being purely a pre-processing step. It has the following characteristics: (i) it can be applied to complete recordings, hence does not require the isolation of primary reflections in the data, (ii) no assumptions are imposed on the subsurface and (iii) it is applicable to multicomponent data. The procedure is based on reciprocity of the medium response, so that differences between normal and reciprocal traces can be attributed to source and receiver perturbations. The application of reciprocity requires symmetric data acquisition, that is, identical source and receiver patterns, identical locations, and the source orientations have to be identical to the receiver components. Besides reciprocity, additional constraints are required to determine the lateral source and receiver amplitude variations fully. We use criteria based on minimizing total energy differences between adjacent common source and common receiver gathers, and in common offset panels of the medium response. Synthetic tests demonstrate that acquisition-related amplitude differences can be significantly reduced using this method.

Key words: AVO, deconvolution, inversion, land seismics, multicomponent, reciprocity.

1 INTRODUCTION

Amplitude anomalies of reflections in seismic recordings have been used for many decades. Initially, the focus was the search for high-intensity seismic reflections, so-called bright spots, in stacked seismic sections. These bright spots could indicate hydrocarbon accumulations, particularly gas. An important development was the introduction of amplitude-versus offset (AVO) interpretation techniques (Ostrander 1984), where observations of reflection coefficients for different angles of incidence can be used to discriminate different lithologies. This allows the separation of gas- and non-gas-related amplitude anomalies. Other applications are the detection of oil reservoirs and of porosity in carbonates (Castagna & Backus 1993).

However, before we can interpret amplitudes in recorded data, we have to compensate for near-surface and acquisition-related effects, such as source strength and receiver coupling variations, preferably in the early stages of the processing. These variations influence all common-midpoint (CMP) based processing, since traces with different sources and receivers are combined in a CMP stack. This degrades the quality of the stack and could lead to biased AVO trends, particularly when related to slowly varying near-surface conditions.

For multicomponent data, it is important to realize that acquisition-related perturbations distort the vector-wavefield characteristics, since coupling has a different effect on horizontal and vertical source and receiver components (Krohn 1984). This can bias the observed polarization (Li & MacBeth 1997; Michaud & Snieder 2004). For example, determining the polarization direction

of the leading split shear wave involves simultaneous rotation of the horizontal source and receiver coordinates to conform with the principal axes of an azimuthal anisotropic medium (Alford 1986). This can only be achieved after separating the acquisition-related amplitude effects on the different recorded wavefield components from the medium response effects.

Amplitude corrections can be performed using surface-consistent processing techniques (Taner & Koehler 1981; Levin 1989; Cambois & Stoffa 1992; Cary & Lorentz 1993). Surface consistency refers to the following approximations: the source and receiver amplitude terms can be expressed as finite-impulse response filters, which do not vary throughout the recording time and are independent of the direction of propagation of the incident wavefield. These existing techniques are applicable to primary reflections which have to be isolated in the data, and common-depth point (CDP) gathering is assumed to be valid. The isolation of primary reflections requires the suppression of ground roll and multiples, which is commonly performed using multichannel filter operations. However, the performance of these multichannel filter operations rapidly deteriorates in presence of amplitude and phase perturbations as a result of the wavefield acquisition. This was already recognized decades ago by Newman & Mahoney (1973), who demonstrated that the performance of source and receiver arrays is sensitive to source and receiver perturbations. Therefore, it is not surprising that careful pre-processing is required before multiples can be successfully eliminated (Kelamis & Verschuur 2000).

We developed an alternative approach to compensate for source and receiver perturbations which is essentially a pre-processing step. It takes full seismic waveforms into account, and does not require mid-point binning. The approach uses reciprocity of the medium response for evaluating lateral source and receiver amplitude variations: differences between normal and reciprocal traces can be attributed to differences in source strength and receiver coupling. Karrenbach (1994) and Luo & Li (1998) applied this technique to determine the seismic source wavelets, assuming that there are no lateral variations in receiver coupling. We show how the latter constraint can be relaxed. This method is also suitable for application to multicomponent data for which the conventional methods cited above often fail because it is more difficult to identify and isolate primary reflections.

Application of reciprocity requires symmetric data acquisition. This includes identical source and receiver positions and shot/receiver patterns, and identical source and receiver components. Multicomponent recordings require thus repeated experiments with horizontal and vertical vibrators.

This paper focuses on the theoretical development and validation of the methodology. van Vossen *et al.* (2006) present a field data application of the developed method.

2 BACKGROUND THEORY: CONVOLUTIONAL MODEL AND RECIPROCITY

Multicomponent data ($3C \times 3C$), excited by sources located at \mathbf{x}_j and recorded at location \mathbf{x}_i , can be represented as a matrix of traces (Auld 1973; Alford 1986; Tatham & McCormack 1991):

$$\mathbf{V}(t, i, j) = \begin{pmatrix} V_{xx}(t, i, j) & V_{xy}(t, i, j) & V_{xz}(t, i, j) \\ V_{yx}(t, i, j) & V_{yy}(t, i, j) & V_{yz}(t, i, j) \\ V_{zx}(t, i, j) & V_{zy}(t, i, j) & V_{zz}(t, i, j) \end{pmatrix}, \quad (1)$$

with the top row corresponding to the in-line (x) geophone traces from in-line (x), crossline (y) and vertical (z) sources. The second row contains crossline geophone traces, and the third row vertical geophone traces. We assume that the source and receiver positions are located on a line. The indices i and j refer to the receiver and source location numbers, respectively.

Considering the Earth as a linear system for the propagation of seismic waves, the recorded traces $\mathbf{V}(t, i, j)$ satisfy the convolutional model (Wapenaar *et al.* 1990),

$$\mathbf{V}(t, i, j) = \mathbf{R}(t, i) * \mathbf{G}(t, i, j) * \mathbf{S}(t, j), \quad (2)$$

where $\mathbf{R}(t, i)$ is the receiver response at surface location \mathbf{x}_i , $\mathbf{S}(t, j)$ is the source signature at surface position \mathbf{x}_j , and $\mathbf{G}(t, i, j)$ is the corresponding medium response. The asterisk (*) denotes convolution in the time domain.

We assume that $\mathbf{R}(t, i)$ and $\mathbf{S}(t, j)$ are surface consistent. This means that effects associated with a particular source or receiver remain constant throughout the recording time, and affect all wave types similarly, regardless of the direction of propagation. The time dependence in $\mathbf{R}(t, i)$ and $\mathbf{S}(t, j)$ denotes the length of the finite-impulse response filters. We also assume that sources and geophones are perfectly aligned, and that crosscoupling between different source and receiver components can be neglected. Then, the geophone and source responses $\mathbf{R}(t, i)$ and $\mathbf{S}(t, j)$ are diagonal matrices of time series with the principal components given by the scalar functions of the in-line, crossline, and vertical geophones and sources.

The objective at this stage is to determine the medium response $\mathbf{G}(t, i, j)$, or to remove the influence of lateral source and receiver variations from the recorded data. To achieve this, we have to determine the individual components in the convolutional model (eq. 2). We can reduce the number of unknown parameters using reciprocity. Because the medium response is reciprocal, differences between recordings of a reciprocal source/receiver pair can be attributed to lateral differences in source strength and receiver coupling. Reciprocity of the medium response is expressed as (Knopoff & Gangi 1959; White 1960):

$$\mathbf{G}(t, i, j) = \mathbf{G}^T(t, j, i), \quad (3)$$

where \mathbf{G}^T is the transpose of \mathbf{G} . Reciprocity can only be applied to data if symmetry conditions are satisfied during data acquisition: the source positions should be identical to the receiver positions, and application of reciprocity to multicomponent recordings thus requires repeated experiments with horizontal and vertical vibrators.

3 FORMULATION OF THE INVERSE PROBLEM

Let us consider an acquisition geometry with N coinciding source/receiver positions. Then, the convolutional model and reciprocity result in a system of equations which constrain the individual terms in the convolutional model. Similar to surface-consistent deconvolution, we can formulate a linear inverse problem in the log/Fourier domain (Taner & Koehler 1981; Cambois & Stoffa 1992). The log/Fourier transform of a time function $X(t)$ is defined as

$$\tilde{X}(\omega) = \log \left[\int_{-\infty}^{\infty} X(t) e^{-i\omega t} dt \right], \quad (4)$$

where log denotes the complex natural logarithm. The inverse transform is defined by:

$$X(t) = \frac{1}{2\pi} \int_{-\infty}^{\infty} e^{\tilde{X}(\omega) + i\omega t} d\omega. \quad (5)$$

Since convolution in the time domain is equivalent to summation in the log/Fourier domain, the convolutional model becomes in the log/Fourier domain:

$$\tilde{\mathbf{V}}(\omega, i, j) = \tilde{\mathbf{R}}(\omega, i) + \tilde{\mathbf{G}}(\omega, i, j) + \tilde{\mathbf{S}}(\omega, j), \quad (6)$$

where the components of $\tilde{\mathbf{V}}(\omega, i, j)$ are the log/Fourier transform of the components of $\mathbf{V}(t, i, j)$:

$$\tilde{\mathbf{V}}(\omega, i, j) = \begin{pmatrix} \tilde{V}_{xx}(\omega, i, j) & \tilde{V}_{xy}(\omega, i, j) & \tilde{V}_{xz}(\omega, i, j) \\ \tilde{V}_{yx}(\omega, i, j) & \tilde{V}_{yy}(\omega, i, j) & \tilde{V}_{yz}(\omega, i, j) \\ \tilde{V}_{zx}(\omega, i, j) & \tilde{V}_{zy}(\omega, i, j) & \tilde{V}_{zz}(\omega, i, j) \end{pmatrix}. \quad (7)$$

The real part of eq. (6) describes the decomposition of the natural logarithm of the Fourier amplitude spectra into the source, receiver, and medium response terms, whereas the imaginary part of eq. (6) gives the decomposition of the phase. In the following, we only consider the amplitude component of the problem.

For the analysis of the system of equations, it is convenient to recast eq. (6) in a matrix-vector form:

$$\mathbf{d}(\omega) = \mathbf{A}\mathbf{m}(\omega), \quad (8)$$

where \mathbf{A} is the coefficient matrix, $\mathbf{m}(\omega)$ contains the unknown parameters in the log/Fourier domain, and the data-vector $\mathbf{d}(\omega)$ contains the measurements of the wavefield $\tilde{\mathbf{V}}(\omega, i, j)$. The model vector $\mathbf{m}(\omega)$ is partitioned into the individual components:

$$\mathbf{m}(\omega) = (\mathbf{m}_G^T(\omega) \mathbf{m}_R^T(\omega) \mathbf{m}_S^T(\omega))^T, \quad (9)$$

where $\mathbf{m}_G(\omega)$ contains the medium response, $\mathbf{m}_R(\omega)$ the receiver terms, and $\mathbf{m}_S(\omega)$ the source wavelets. The coefficient matrix \mathbf{A} is frequency independent. It only contains ones and zeros. We give an example for the structure of the coefficient matrix for single component data in Appendix A.

We treat reciprocity of the medium response as an exact relationship. Instead of inserting the reciprocal eq. (3) in the coefficient matrix \mathbf{A} , we directly reduce the number of unknown parameters in $\mathbf{m}_G(\omega)$ by explicitly substituting the reciprocal medium response terms using eq. (3). Since the number of unknowns is reduced, this approach is computationally favourable.

Furthermore, we can only solve for relative source and receiver differences. Consequently, we can impose a zero-mean constraint on the source and receiver terms without loss of generality. We also treat this as an exact relationship and implement it in a similar fashion as the reciprocity constraints.

4 ANALYSIS OF RECIPROCITY CONSTRAINTS ON SINGLE COMPONENT DATA

In this section we analyse the constraints on the source, receiver and medium response terms using single component data. We use singular value decomposition (Lanczos 1961) to analyse these constraints on the model parameters. Consider a source and receiver array with $N = 41$ coinciding source and receiver positions. For $N > 5$, there are more data $N_D = N^2$ than unknown parameters $N_U = (N + 1)N/2 + 2(N - 1)$: \mathbf{m}_G has $(N + 1)N/2$ unknown coefficients, and both \mathbf{m}_R and \mathbf{m}_S contain $N - 1$ unknown terms. In this example, there are 941 unknown parameters. The singular values of \mathbf{A} are shown in Fig. 1. There are $N - 1$ zero singular values, thus $N - 1$ degrees of freedom in the inverse problem.

In order to gain more insight in the nullspace of the inverse problem, we consider the following equations for a reciprocal source–

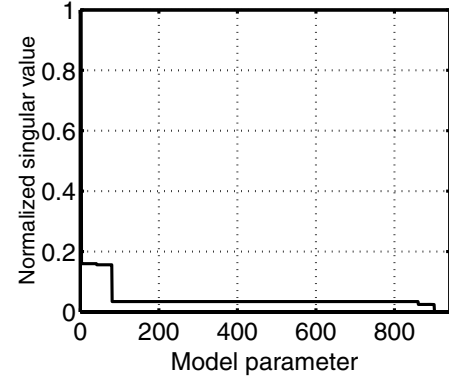


Figure 1. Normalized singular values for reciprocity/convolutional model inversion with $N = 41$ source/receiver positions. There are 941 model parameters in this example, and $N - 1$ zero singular values, thus $N - 1$ remaining degrees of freedom.

receiver pair:

$$\tilde{V}(\omega, i, j) = \tilde{R}(\omega, i) + \tilde{G}(\omega, i, j) + \tilde{S}(\omega, j), \quad (10)$$

$$\tilde{V}(\omega, j, i) = \tilde{R}(\omega, j) + \tilde{G}(\omega, i, j) + \tilde{S}(\omega, i), \quad (11)$$

where the indices $i, j = 1, \dots, N$. Subtracting eq. (11) from (10) and adding eq. (11) to (10) yield the following two equations:

$$\begin{aligned} \tilde{V}(\omega, i, j) - \tilde{V}(\omega, j, i) &= (\tilde{R}(\omega, i) - \tilde{S}(\omega, i)) \\ &\quad - (\tilde{R}(\omega, j) - \tilde{S}(\omega, j)), \end{aligned} \quad (12)$$

$$\begin{aligned} \tilde{V}(\omega, i, j) + \tilde{V}(\omega, j, i) &= (\tilde{R}(\omega, i) + \tilde{S}(\omega, i)) \\ &\quad + (\tilde{R}(\omega, j) + \tilde{S}(\omega, j)) \\ &\quad + 2\tilde{G}(\omega, i, j). \end{aligned} \quad (13)$$

Eq. (12) shows that the differences $\tilde{R}(\omega, i) - \tilde{S}(\omega, i)$ are constrained up to a constant (one remaining degree of freedom) when at least three coinciding sources and receivers are used, that is, when $N > 3$. However, the sum $\tilde{R}(\omega, i) + \tilde{S}(\omega, i)$ cannot be determined using reciprocity constraints. Eq. (13) shows that there is a trade-off between the obtained responses for the Green's functions $\tilde{G}(\omega, i, j)$ and the sum of the source and receiver responses at surface locations i and j . Thus, given the reciprocity constraints, the number of degrees of freedom is equal to the number of sources or receivers $N + 1$. Since we only solve for relative source and receiver perturbations, the number of degrees of freedom in the inverse problem reduces to $N - 1$. Hence, additional information is required to obtain a unique solution to the inverse problem.

5 REGULARIZATION CRITERIA

We investigate regularization using energy criteria and minimum variation in common-offset sections of the medium response. Energy criteria give prior information on the source and receiver terms, and the variation criterion provides information about the medium response. Prior information (or the reference model), denoted by \mathbf{m}^0 , is included in the inverse problem defining a cost function:

$$Y = (\mathbf{A}\mathbf{m} - \mathbf{d})^T \mathbf{C}_d^{-1} (\mathbf{A}\mathbf{m} - \mathbf{d}) + (\mathbf{m} - \mathbf{m}^0)^T \mathbf{C}_m^{-1} (\mathbf{m} - \mathbf{m}^0), \quad (14)$$

where \mathbf{C}_d^{-1} is the inverse of the data covariance matrix which we take to be diagonal, and \mathbf{C}_m^{-1} is the inverse of the prior model covariance

matrix. It is a block-diagonal matrix and can be written in partitioned form:

$$\mathbf{C}_m^{-1} = \begin{pmatrix} \mathbf{C}_{m_G}^{-1} & \mathbf{0} & \mathbf{0} \\ \mathbf{0} & \mathbf{C}_{m_R}^{-1} & \mathbf{0} \\ \mathbf{0} & \mathbf{0} & \mathbf{C}_{m_S}^{-1} \end{pmatrix}, \quad (15)$$

where \mathbf{C}_{m_G} , \mathbf{C}_{m_R} and \mathbf{C}_{m_S} are the covariance matrices describing prior information on the medium response, receiver, and source terms, respectively. The least squares solution of eq. (14) is found by setting the derivatives with respect to the model parameters equal to zero, and is given by (e.g. Tarantola 1987):

$$\tilde{\mathbf{m}} = (\mathbf{A}^T \mathbf{C}_d^{-1} \mathbf{A} + \mathbf{C}_m^{-1})^{-1} (\mathbf{A}^T \mathbf{C}_d^{-1} \mathbf{d} + \mathbf{C}_m^{-1} \mathbf{m}^0). \quad (16)$$

The model resolution matrix is then:

$$\mathbf{R} = (\mathbf{A}^T \mathbf{C}_d^{-1} \mathbf{A} + \mathbf{C}_m^{-1})^{-1} \mathbf{A}^T \mathbf{C}_d^{-1} \mathbf{A}. \quad (17)$$

The resolution operator tells us to what extent we can retrieve the chosen model parameters independently from the inverse operator. The total number of independent parameters used to construct the estimated model is given by the trace of the resolution matrix.

An alternative approach is to add information only to the nullspace of the unregularized inversion. The procedure of adding nullspace information while retaining the data fit was originally proposed by Deal & Nolet (1996) for tomographic inverse problems. We consider this approach less flexible in dealing with data contaminated by noise, and therefore we only show results for the conventional implementation using regularization criteria shown in eq. (16).

In the following sections we show that prior information given by a minimum variation criterion and energy criteria can be incorporated in the conventional formalism, that is, we derive expressions for the prior model and for the prior model covariances for the proposed regularization criteria. The derivations are given for single component data, but are readily generalized for multicomponent data.

5.1 Minimum variation in common-offset domain

Prior information on the medium response can be obtained by minimizing variation in common-offset sections of the medium response. It follows from the convolutional model that insufficient corrections for the source and receiver variations result in perturbations of the medium response. This causes larger variation in common-offset sections of the medium response. Thus, if we correctly retrieve these lateral source and receiver variations, the amplitude variations in the common-offset sections of the medium response are reduced to the minimum required by the data.

We define variation in the common-offset medium response using a measure of length (Menke 1984):

$$\begin{aligned} L(\mathbf{x}_o) &= [\mathbf{m}_G(\mathbf{x}_o) - \boldsymbol{\mu}_G(\mathbf{x}_o)]^T [\mathbf{m}_G(\mathbf{x}_o) - \boldsymbol{\mu}_G(\mathbf{x}_o)] \\ &= [\mathbf{A}_l(\mathbf{x}_o) \mathbf{m}_G(\mathbf{x}_o)]^T [\mathbf{A}_l(\mathbf{x}_o) \mathbf{m}_G(\mathbf{x}_o)], \end{aligned} \quad (18)$$

where $\mathbf{m}_G(\mathbf{x}_o)$ denotes the partition of \mathbf{m}_G with offset \mathbf{x}_o , and the elements of $\boldsymbol{\mu}_G(\mathbf{x}_o)$ are the average of $\mathbf{m}_G(\mathbf{x}_o)$:

$$[\boldsymbol{\mu}_G(\mathbf{x}_o)]_j = \frac{\sum_{i=1}^{N(\mathbf{x}_o)} [m_G(\mathbf{x}_o)]_i}{N(\mathbf{x}_o)}, \quad j = 1, \dots, N(\mathbf{x}_o), \quad (19)$$

with $N(\mathbf{x}_o)$ the number of traces with offset \mathbf{x}_o . The matrix $\mathbf{A}_l(\mathbf{x}_o)$ is the coefficient matrix, and is defined such that $\mathbf{A}_l(\mathbf{x}_o) \mathbf{m}_G(\mathbf{x}_o) = \mathbf{m}_G(\mathbf{x}_o) - \boldsymbol{\mu}_G(\mathbf{x}_o)$.

We define the minimum variation cost function L by combining all common-offset sections, using the number of traces in each

common-offset section as weights, that is, this criterion provides more reliable information using common-offset sections with many traces, since the mean value and variation with respect to this mean value can be determined more accurately. The cost function is given by:

$$L = \sum_{\mathbf{x}_o} N(\mathbf{x}_o) L(\mathbf{x}_o) = [\mathbf{A}_l \mathbf{m}_G]^T \mathbf{W}_m [\mathbf{A}_l \mathbf{m}_G(\omega)]. \quad (20)$$

The coefficient matrix \mathbf{A}_l comprises all individual matrices $\mathbf{A}_l(\mathbf{x}_o)$, and the diagonal matrix \mathbf{W}_m contains the corresponding weighting factors $N(\mathbf{x}_o)$ and is normalized such that the maximum value of

$$\max [\mathbf{A}_l^T \mathbf{W}_m \mathbf{A}_l] = \frac{2}{N+1}. \quad (21)$$

This maximum is set equal to the ratio of the number of unknowns in \mathbf{m}_R or \mathbf{m}_S over \mathbf{m}_G . This normalization has been chosen to reduce the dependency of the damping parameters on the number of sources/receivers.

The minimum variation criterion can be included in the inverse problem (eq. 14), with the inverse of the medium-response model covariance given by:

$$\mathbf{C}_{m_G}^{-1} = \theta \mathbf{A}_l^T \mathbf{W}_m \mathbf{A}_l, \quad (22)$$

where θ is the overall damping parameter. We set the prior medium response

$$\mathbf{m}_G^0 = \mathbf{0}. \quad (23)$$

The choice of the prior medium responses do not influence the inversion results when these are set to a constant value. This criterion minimizes differences with respect to the average value in common offset panels.

5.2 Energy criteria

Consider a common source gather for a source positioned at \mathbf{x}_j with N receivers. The energy for frequency ω in this gather is proportional to the squared sum of all traces:

$$E(\omega, j) = \sum_{i=1}^N |v(\omega, i, j)|^2. \quad (24)$$

Inserting the convolutional model (eq. 2) into eq. (24) yields:

$$E(\omega, j) = |S(\omega, j)|^2 \left(\sum_{i=1}^N |R(\omega, i)|^2 |G(\omega, i, j)|^2 \right). \quad (25)$$

The energy in the common source gathers for the adjacent source position, with geophones positioned at similar offsets, is given by:

$$\begin{aligned} E(\omega, j+1) &= |S(\omega, j+1)|^2 \\ &\times \left(\sum_{i=1}^N |R(\omega, i+1)|^2 |G(\omega, i+1, j+1)|^2 \right). \end{aligned} \quad (26)$$

For closely spaced sources, we may assume that differences in the medium response only occur close to these sources. Consequently, energy differences between two adjacent common source gathers are primarily due to differences at the source. This leads to the following approximation for the energy difference between two adjacent

common source gathers:

$$\begin{aligned}
 E(\omega, j+1) - E(\omega, j) &\approx [|S(\omega, j+1)|^2 - |S(\omega, j)|^2] \\
 &\times \frac{1}{2} \left\{ \sum_{i=1}^N |R(\omega, i)|^2 |G(\omega, i, j)|^2 \right. \\
 &\left. + |R(\omega, i+1)|^2 |G(\omega, i+1, j+1)|^2 \right\}. \quad (27)
 \end{aligned}$$

The last term in eq. (27) is the average of the medium response and the receiver terms of the two adjacent common source gathers (eqs 25 and 26). It is assumed that this accurately represents the medium and receiver responses for both sources.

Using a similar approximation for $E(\omega, j+1) + E(\omega, j)$, we obtain for the division of the energy difference by its sum:

$$\frac{E(\omega, j+1) - E(\omega, j)}{E(\omega, j+1) + E(\omega, j)} \approx \frac{|S(\omega, j+1)|^2 - |S(\omega, j)|^2}{|S(\omega, j+1)|^2 + |S(\omega, j)|^2}. \quad (28)$$

Eq. (28) is equivalent to

$$|S(\omega, j+1)|^2 - \frac{E(\omega, j+1)}{E(\omega, j)} |S(\omega, j)|^2 = 0. \quad (29)$$

We obtain expressions in the log/Fourier domain by taking the natural logarithm of eq. (29):

$$\tilde{S}(\omega, j+1) - \tilde{S}(\omega, j) = \frac{1}{2} \log \left[\frac{E(\omega, j+1)}{E(\omega, j)} \right], \quad (30)$$

where the energy term on the right of eq. (30) is calculated from the data alone. Hence, this equation imposes additional data-derived constraints on the source terms. Since we can only solve for relative source variations, we can impose a zero-mean constraint on the source terms. This imposes an artificial absolute scale on the Green's functions which is always required in seismic data processing. Eq. (30) can be written in matrix-vector form:

$$\mathbf{A}_0 \mathbf{m}_S^0(\omega) = \mathbf{d}_S^0(\omega), \quad (31)$$

where $\mathbf{m}_S^0(\omega)$ contains the prior source variations, $\mathbf{d}_S^0(\omega)$ is the data vector, and \mathbf{A}_0 is the coefficient matrix. We obtain the prior model estimate for \mathbf{m}_S^0 using the least-squares solution of eq. (31).

A similar analysis can be performed in the common receiver domain. This results in the following system of equations for the prior receiver terms:

$$\tilde{R}(\omega, i+1) - \tilde{R}(\omega, i) = \frac{1}{2} \log \left[\frac{E(\omega, i+1)}{E(\omega, i)} \right]. \quad (32)$$

Eq. (32) in matrix-vector form is written as:

$$\mathbf{A}_0 \mathbf{m}_R^0(\omega) = \mathbf{d}_R^0(\omega), \quad (33)$$

where $\mathbf{m}_R^0(\omega)$ contains the prior receiver model parameters, and $\mathbf{d}_R^0(\omega)$ is the data vector.

We use the covariance matrices \mathbf{C}_{m_R} and \mathbf{C}_{m_S} to impose the energy criteria upon the model vector. We define these as:

$$\mathbf{C}_{m_R}^{-1} = \frac{2\theta\phi\lambda \mathbf{A}_0^T \mathbf{A}_0}{\max[\mathbf{A}_0^T \mathbf{A}_0]}, \quad (34)$$

$$\mathbf{C}_{m_S}^{-1} = \frac{2\theta\phi(1-\lambda) \mathbf{A}_0^T \mathbf{A}_0}{\max[\mathbf{A}_0^T \mathbf{A}_0]}, \quad (35)$$

where θ is the overall damping parameter. The smaller the value of θ , the more the model parameters are allowed to vary around

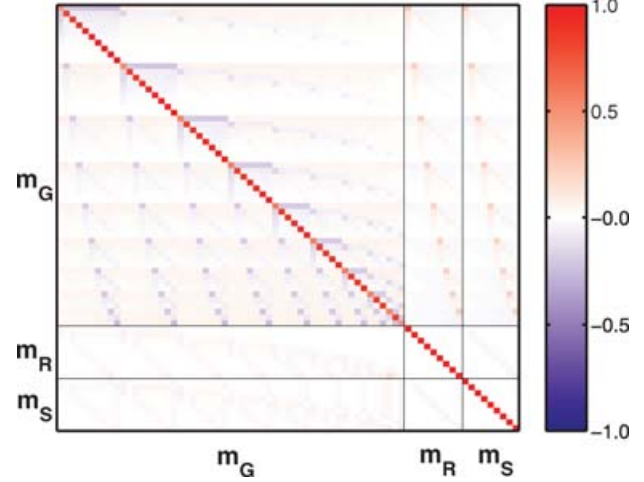


Figure 2. Model resolution matrix for data acquired with $N = 11$ coinciding sources and receivers. The ordering of the model parameters is explained in Appendix A.

the energy and minimum variation constraints, and the better the data can be explained. The parameter ϕ determines the strength of the energy criteria relative to the variation criterion, and λ controls the relative strength of the energy criteria applied in the common source domain compared to the common receiver domain, and may take values between 0 and 1. The denominator in eqs (34) and (35) is used to reduce the dependency of the damping parameters ϕ and λ on the number of sources/receivers considered in the inverse problem.

5.3 Resolution of regularized inverse problem

An example of the model resolution matrix \mathbf{R} of the regularized inverse problem (eq. 17) is shown in Fig. 2. It is computed for a system of constraints obtained with $N = 11$ sources and single component receivers. The values of the damping parameters were: $\theta = 0.001$, $\phi = 0.5$ and $\lambda = 0.5$, respectively. The ordering of the model parameters is explained in Appendix A.

The resolution matrix shows that the source and receiver terms are best resolved, whereas the Green's functions have larger trade-offs. Note that the trade-offs are largest for the zero-offset Green's functions. This is a result of the absence of reciprocity constraints on zero-offset data.

6 SYNTHETIC EXAMPLE

We illustrate the method with a synthetic example on single component data, and analyse the influence of the selection of the damping parameters.

6.1 Data description

Consider the model shown in Fig. 3 with a synclinal structure and lateral heterogeneity close to the free surface. The model parameters are listed in Table 1. Synthetic data were computed with a viscoelastic finite-difference code (Robertsson *et al.* 1994). The first source and receiver are positioned at 100 m, the last ones at 900 m. The shot and receiver spacing is 20 m: there are 41 source and receiver positions. Both sources and receivers are located at the free surface. The

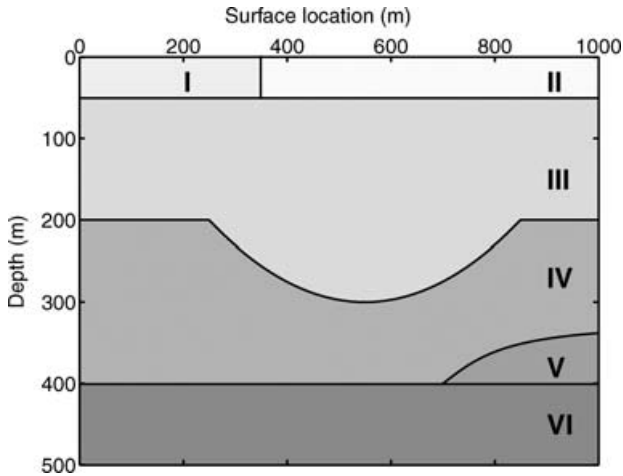


Figure 3. Synclinal model used to generate synthetic data, with layers numbered for identification.

Table 1. Values for velocity, density, and attenuation for each layer in the model shown in Fig. 3.

Layer number	α (m s ⁻¹)	β (m s ⁻¹)	ρ (kg m ⁻³)	Q_p	Q_s
I	1100	280	1700	100	50
II	900	250	1700	100	50
III	1500	400	2000	10 000	10 000
IV	2200	600	2100	10 000	10 000
V	2500	700	2150	10 000	10 000
VI	3000	800	2200	10 000	10 000

source mechanism is a vertical force source, which emits a Ricker wavelet with a 40 Hz central frequency. The time sampling interval is 0.001 s, and a trace has 4000 samples.

Two common-offset panels of the data are shown in Fig. 4. The ground-roll is the most energetic event in the data. The near-surface lateral heterogeneity results in different amplitudes and traveltimes in the *P*-*P* reflected waves between 0.10 and 0.20 s, and causes backscattering of surface waves. These are the events with the high-moveout velocities in the zero-offset section. The synclinal structure is easily recognized in the zero-offset panel. The structure is repeated due to reverberations in the near-surface low-velocity layer. The 200 m common-offset panel shows that the near-surface heterogeneity results in different moveout velocities for the ground

Table 2. Values for average resonant frequencies and damping factors of source and receiver perturbations and the standard deviations.

	f_c (Hz)	f_g (Hz)	f_s (Hz)	η_c	η_g	η_s
μ	120	4.5	120	1.0	1.0	0.8
σ	40	0.5	40	0.2	0.2	0.2

roll, which are the large amplitude events between 0.8 and 1.0 s. The signature of the synclinal structure is less pronounced in these data.

At the receiver side, data are perturbed using a damped harmonic oscillator description. This represents both the response of the geophone-ground coupling, and of the instrument response (Hoover & O'Brien 1980; Krohn 1984). The complex response can be written as:

$$R(f) = \frac{-\left(\frac{f}{f_g}\right)^2 [1 + i\left(\frac{f}{f_c}\right)\eta_c]}{\left[1 - \left(\frac{f}{f_g}\right)^2 + i\left(\frac{f}{f_g}\right)\eta_g\right] \left[1 - \left(\frac{f}{f_c}\right)^2 + i\left(\frac{f}{f_c}\right)\eta_c\right]} \quad (36)$$

In this model, f_g and f_c are the resonant frequencies, and η_g and η_c are the damping factors for the geophone's internal spring, denoted with subscript *g*, and for the geophone ground coupling, indicated with subscript *c*. Critical damping occurs when η_g or $\eta_c = 2$. In this equation, *i* denotes the imaginary unit $\sqrt{-1}$.

We also used a damped harmonic oscillator description to represent the coupling of the source (vertical vibrator) to the ground (Sallas 1984):

$$S(f) = \frac{-[1 + i\left(\frac{f}{f_s}\right)\eta_s]}{\left[1 - \left(\frac{f}{f_s}\right)^2 + i\left(\frac{f}{f_s}\right)\eta_s\right]}, \quad (37)$$

where f_s and η_s are source coupling resonant frequency and damping parameter. For each source and geophone, the resonant frequencies and damping parameters are selected randomly from a Gaussian distribution. The parameters which characterize these distributions are listed in Table 2.

We only used the damped-oscillator description for the source and receiver perturbations in these synthetic examples. The inversion method does not use any constraints that follow from this model, and is thus independent from the damped-oscillator parametrization.

Since we are only able to solve for relative source and receiver perturbations in the log/Fourier domain, we decompose the source

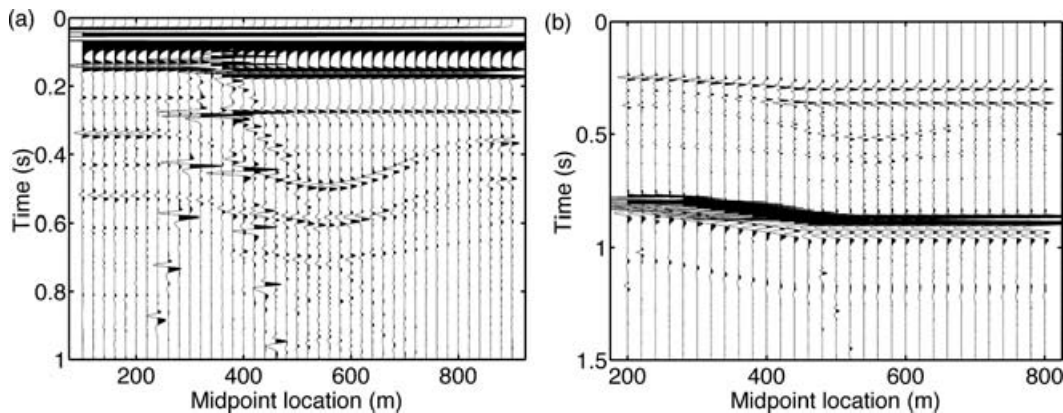


Figure 4. Common-offset panels for (a) 0 m and (b) 200 m offset.

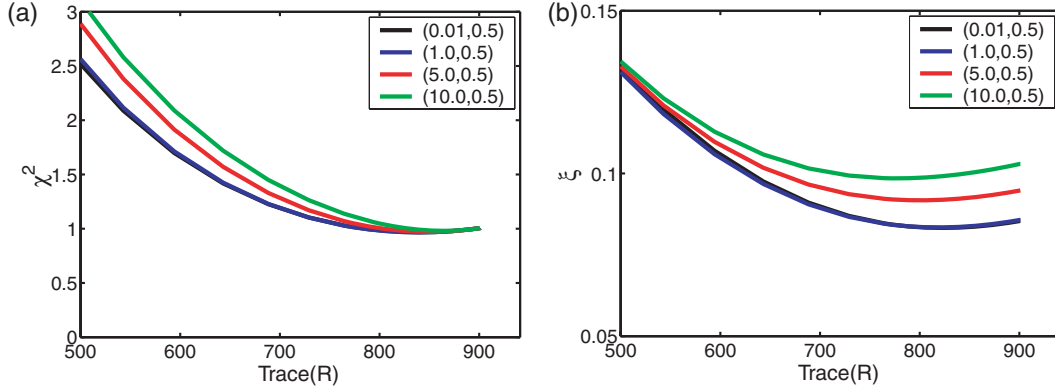


Figure 5. Misfit curves obtained for various source and receiver perturbations. The curves are labelled showing the values of the parameters (ϕ, λ) . (a) shows the data misfit with the reduced chi-squared measure, and (b) shows the true model misfit.

and receiver terms into an average and a perturbation term:

$$R(\omega, i) = \bar{R}(\omega) \left[1 + \frac{\Delta_R(\omega, i)}{\bar{R}(\omega)} \right] = \bar{R}(\omega) \Delta'_R(\omega, i), \quad (38)$$

$$S(\omega, j) = \bar{S}(\omega) \left[1 + \frac{\Delta_S(\omega, j)}{\bar{S}(\omega)} \right] = \bar{S}(\omega) \Delta'_S(\omega, j), \quad (39)$$

where $\bar{R}(\omega)$ is the geometric mean of the different receiver terms:

$$\bar{R}(\omega) = \left[\prod_{i=1}^N R(\omega, i) \right]^{1/N}. \quad (40)$$

The relative source and receiver terms are $\Delta'_S(\omega, j)$ and $\Delta'_R(\omega, i)$, respectively. The geometric mean in the Fourier domain corresponds to the arithmetic mean in the log/Fourier domain. Thus, the arithmetic mean of the relative source and receiver terms $\Delta'_S(\omega, j)$ and $\Delta'_R(\omega, i)$ is zero in the log/Fourier domain.

6.2 Results

We first study inversion results for a single frequency. To gain an idea of the influence of ϕ and λ on the model estimate, we minimize eq. (14) many times, systematically varying the parameters ϕ and λ . We added errors to the data drawn from a Gaussian distribution with a standard deviation $\sigma_d = 0.10$ in the log/Fourier domain. This corresponds to errors with a standard deviation of 10 per cent of the values of the synthetic data in the frequency domain. The experiments are repeated with different manifestations of random noise. We performed experiments for different resonant frequencies and damping parameters for the source and receiver perturbations, and plot the reduced χ^2 as a function of independent parameters in the final model. We define the reduced χ^2 as:

$$\chi^2 = \frac{1}{N_D - M} (\mathbf{A}\mathbf{m} - \mathbf{d})^T \mathbf{C}_d^{-1} (\mathbf{A}\mathbf{m} - \mathbf{d}), \quad (41)$$

where N_D is the number of data and $M = \text{trace}(\mathbf{R})$. Furthermore, we compare the estimated model to the true solution \mathbf{m}_{true} . We quantify the true-model misfit with

$$\xi^2 = \frac{(\hat{\mathbf{m}} - \mathbf{m}_{\text{true}})^T (\hat{\mathbf{m}} - \mathbf{m}_{\text{true}})}{N_U}, \quad (42)$$

where N_U is the number of unknown parameters. The measure ξ has been chosen such that it can be interpreted as an average uncertainty in the estimated model parameters.

Fig. 5 shows misfit curves for the data and model uncertainty for $f = 50$ Hz. These misfit curves are computed varying the overall damping parameter θ , and consequently the trace of \mathbf{R} using eq. (17). If we reduce the overall damping θ , that is, allowing more independent parameters in the inversion, the data are better explained, resulting in small values for χ^2 . As we reduce the overall damping, χ^2 monotonically tends towards 1, as expected.

Both the data and the model misfit measures indicate that best results are obtained if $\phi \leq 1$. For a fixed value of trace (\mathbf{R}), the data are better explained for $\phi \leq 1$. For larger values, both the data and model misfit increase. Thus, the source and receiver terms are better constrained by the data than the individual medium response terms, that is, all equations in a common source gather constrain the individual source term, whereas there is only one equation for a particular Green's function. Hence, imposing prior information on the source and receiver terms potentially has a larger influence on data and model misfit than prior information on the medium response terms. Sensitivity tests for λ , the trade-off parameter between source and receiver terms, indicated that the inversion results are not influenced by variations in this parameter.

An example of the inversion for lateral source and receiver perturbations is shown in Fig. 6. In Fig. 6(a), the ordinate value R_{zz} represents the vertical component of the receiver correction, and S_{zz} in Fig. 6(b) represents the vertical component of the source correction. The frequency $f = 50$ Hz, and the damping parameter values are $\theta = 0.001$, $\phi = 0.01$ and $\lambda = 0.5$, resulting in trace (\mathbf{R}) ≈ 901 . Inversion results are shown for data without additional Gaussian noise, and for data contaminated with additional Gaussian noise with standard deviation 0.10. In order to quantify the error, we use the measure $\xi_{R,S}$ for the source and receiver amplitude terms:

$$\xi_{R,S}^2 = \frac{(\hat{\mathbf{m}}_R - \mathbf{m}_{R\text{true}})^T (\hat{\mathbf{m}}_R - \mathbf{m}_{R\text{true}}) + (\hat{\mathbf{m}}_S - \mathbf{m}_{S\text{true}})^T (\hat{\mathbf{m}}_S - \mathbf{m}_{S\text{true}})}{2N}. \quad (43)$$

For the data without additional Gaussian noise, there is a good fit to the reference solution, which is the true solution for the lateral source and receiver amplitude variations: $\xi_{R,S} = 0.036$. For the data contaminated with the additional Gaussian noise, the fit is slightly less good: $\xi_{R,S} = 0.042$.

Fig. 7 shows inversion results for sources and receivers 10, 20 and 30 as a function of frequency for the data contaminated with the Gaussian noise. The overall trends of the source and receiver

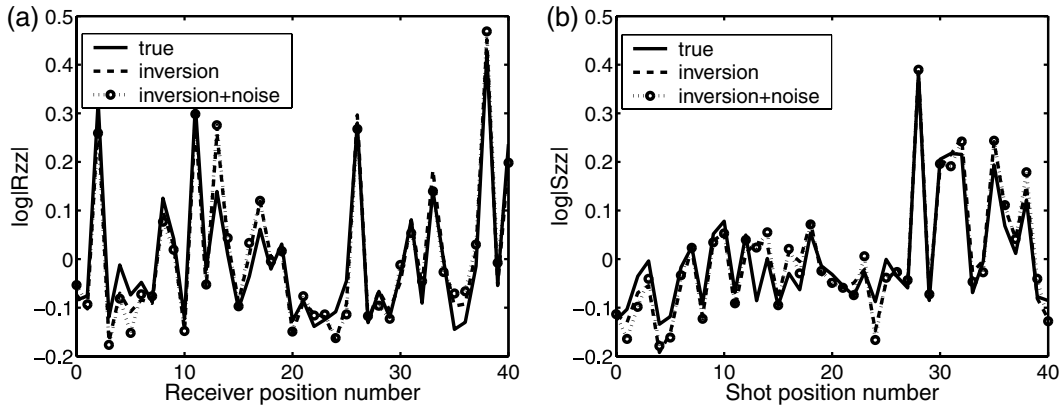


Figure 6. Inversion results for relative (a) receiver and (b) source perturbations at frequency $f = 50$ Hz. The inversion results are computed with the following damping parameter values: $\theta = 0.001$, $\phi = 0.01$, and $\lambda = 0.5$, which results in $\text{trace}(\mathbf{R}) \approx 901$, and are compared to the true solution. Results are shown for unperturbed data, and for data contaminated with 10 per cent Gaussian noise.

perturbations are well resolved, although the inversion results for the different frequencies are scattered around these curves.

Instead of using directly the inversion results for the medium response \mathbf{m}_G , we use the lateral source and receiver terms to compensate the recorded data for these effects. This allows us to use an additional requirement that the source and receiver terms have a finite impulse response (e.g. Drijkoningen 2000). This constraint was not imposed explicitly in our implementation, the presented procedure yields estimates for each frequency independently, and this corresponds to a smoothing operator in the frequency domain. Thus, we use smoothed versions of the source and receiver terms, and these agree well with the source and receiver perturbations added to the data (Fig. 7).

Thus, the compensation scheme consists of the following steps: first we estimate the filters which compensate for lateral source and receiver variations in the log/Fourier domain. These inverse filters are obtained by reversing the sign in the log/Fourier domain. Then, we apply the inverse log/Fourier transform and limit the impulse response in the time domain. This operation is performed such that the resulting filters are zero phase, and the filter length is 0.03 s. Finally, we correct the recorded data for lateral source and receiver amplitude variations by convolution in the time domain.

We illustrate the performance of this compensation scheme on the synthetic data described in the previous section. We added errors drawn from a Gaussian distribution with a standard deviation of 10 per cent of the values of the synthetic data in the time domain, followed by a low-pass filter with 100 Hz cut-off frequency, and use the same values of the damping parameters as in the previous example. Figs 8 and 9 show the results on the recorded zero-offset data. Fig. 8 shows the results of the first arrival. The amplitudes in Fig. 9 are blown up to focus on the reflected waves.

The results are compared to a reference solution which includes the phase shifts induced by the lateral source and receiver variations and the average source and receiver terms. Thus, the reference solution is the input data which are compensated for the lateral source and receiver amplitude variations, and do not contain the additional Gaussian errors. The phase differences are included in the reference solution to be able to demonstrate the performance of the amplitude correction scheme. Otherwise, we would obtain differences between the compensated data and the reference solution due to the phase differences for which we do not compensate.

Both for the first arrival and for the reflected waves, the differences of the corrected solution with the reference solution are

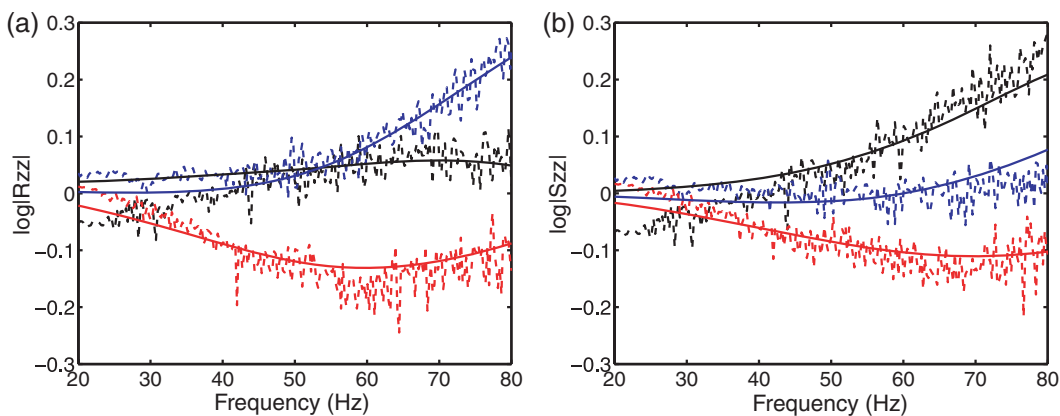


Figure 7. Inversion results for receiver (a) and source (b) perturbations as a function of frequency. Shown are curves for source/receiver positions 10 (black), 20 (blue) and 30 (red). The solid curves represent the true solutions, and the dashed curves are the inversion results. The values for the damping parameters are: $\theta = 0.001$, $\phi = 0.01$, and $\lambda = 0.5$, and the data are contaminated with 10 per cent Gaussian noise.

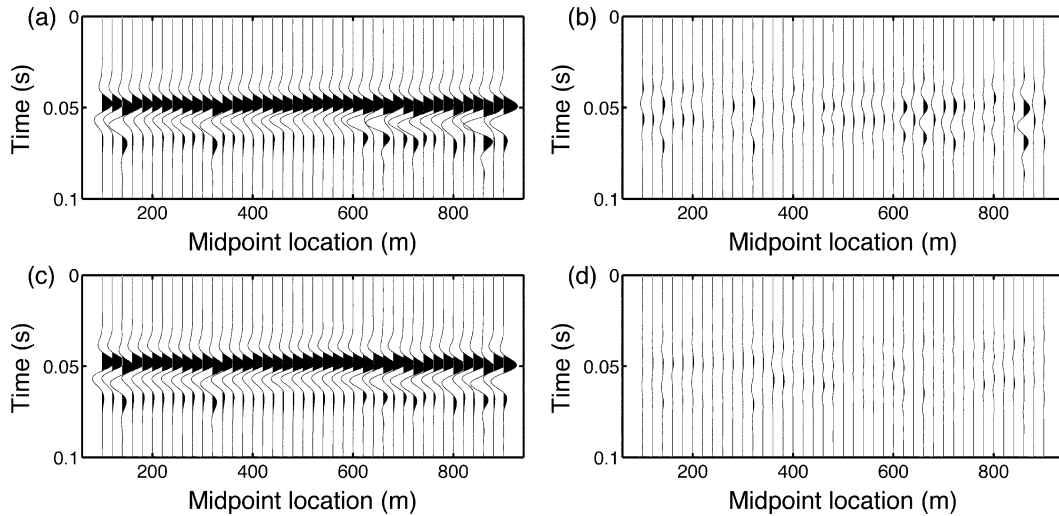


Figure 8. Effect of source and receiver amplitude corrections on zero offset data: focus on ground roll. Shown are (a) perturbed data, (b) difference between perturbed data and reference solution, (c) corrected data and (d) difference between these corrected data and reference solution.

significantly smaller than for the perturbed data. The large errors in the first 0.1 s of Fig. 9(d) correspond to the residue shown in Fig. 8(d).

Similar results are obtained for amplitude corrections for 200 m offset data (Figs 10 and 11). Amplitude errors in both the ground roll and the reflected waves are reduced.

In order to quantify the performance of the amplitude correction scheme, we consider the ratio $\Delta E/E_{\text{ref}}$, where ΔE is the energy of the difference between either the perturbed data or the corrected data and the reference solution, and E_{ref} is the energy of the reference solution. We computed the ratio $\Delta E/E_{\text{ref}}$ using all data traces. For the data considered, this ratio decreases from 0.032 to 0.0049

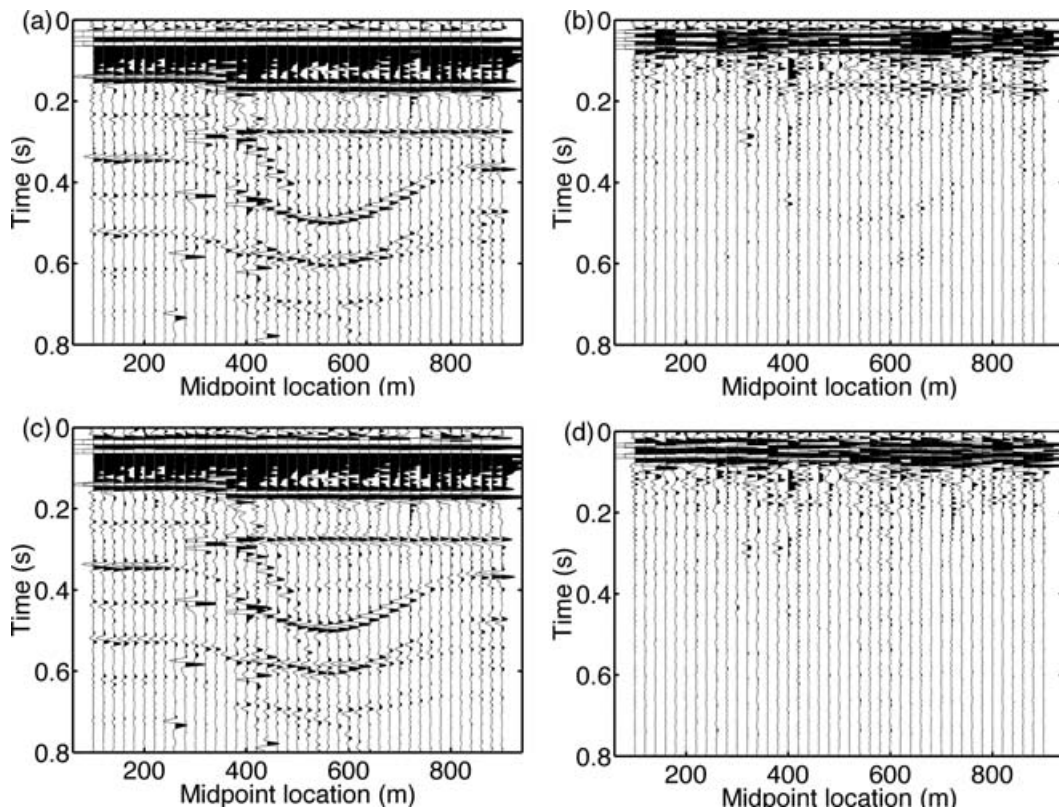


Figure 9. Effect of source and receiver amplitude corrections on zero offset data: focus on reflected waves. Shown are (a) perturbed data, (b) difference between perturbed data and reference solution, (c) corrected data and (d) difference between corrected data and reference solution.

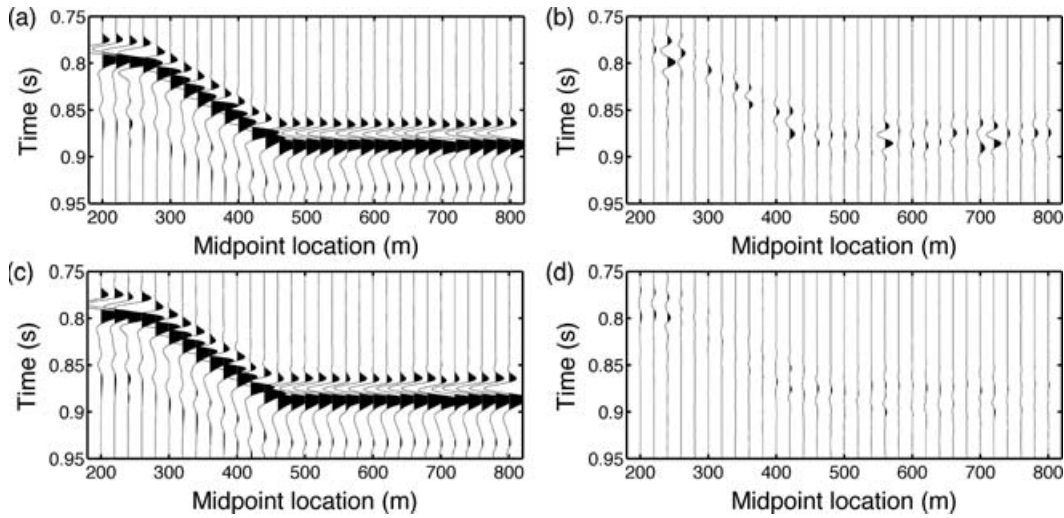


Figure 10. Effect of source and receiver amplitude corrections on 200 m offset data: focus on ground roll. Shown are (a) perturbed data, (b) difference between perturbed data and the reference solution, (c) corrected data and (d) difference between these corrected data and the reference solution.

after applying the corrections for the source and receiver amplitude perturbations.

This synthetic example demonstrates that the proposed technique significantly reduces effects of lateral source and receiver variations from the data, without having to select primary reflections and without prior structural information.

7 DISCUSSION

The correction for lateral source and receiver variations is based on the assumption that the conditions for reciprocity are applicable to seismic data acquisition. In practice, however, positioning of sources and receivers at identical positions is difficult to realize. Moreover,

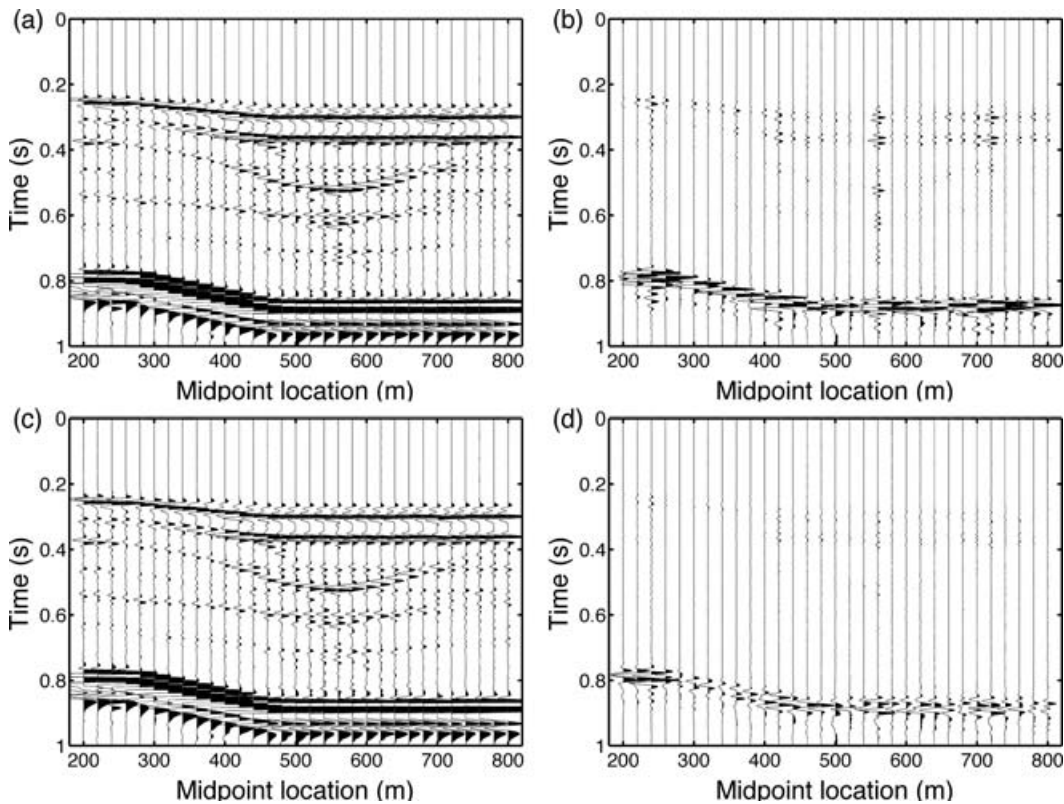


Figure 11. Effect of source and receiver amplitude corrections on 200 m offset data: focus on reflected waves. Shown are (a) perturbed data, (b) difference between perturbed data and the reference solution, (c) corrected data and (d) difference between these corrected data and the reference solution.

we also need to consider an explosive source in addition to a vertical force source (vibrator), and source patterns are also commonly used in land seismics.

Fenati & Rocca (1984) conducted a field test to assess the applicability of reciprocity in the field using both explosive and vibratory sources. They observed a good coherence between the direct and reciprocal traces regardless of the source, except at near offsets and early times with explosive sources. Furthermore, we performed sensitivity tests to evaluate the effect of non-identical source–receiver positions. These tests indicated that the results are not influenced by small differences in source and receiver positions when the distance between the reciprocal sources and receivers remains constant. For example, this allows sources at a shallow depth, while the receivers are positioned at the surface. We also expect that the results are not sensitive to a small displacement between parallel source and receiver lines.

It is important to realize that, contrary to conventional surface-consistent processing techniques (Taner & Koehler 1981; Levin 1989; Cambois & Stoffa 1992; Cary & Lorentz 1993), reciprocity constrains source and receiver effects only, which do not include wavefield propagation effects of the near surface. Thus, we assume that the amplitude perturbations for each source and receiver component are independent of the wave type and the angle of incidence. Since we do not include wavefield propagation effects through the near surface, surface consistency does not assume wave propagation in which seismic energy travels through the near surface along vertical paths, as in static corrections. Therefore, the presence of ground roll in the data will not necessarily violate the surface-consistent assumption.

Application to field data requires the computation of the inverse operator for $(\mathbf{A}^T \mathbf{C}_d^{-1} \mathbf{A} + \mathbf{C}_m^{-1})$ (eq. 16). In practice, however, the matrix will be too big to invert and to retain in memory. In such cases, the data should be decomposed into smaller sets, each of which would be processed separately. This is common practice in conventional surface-consistent processing techniques, and it is argued that this does not degrade the accuracy of the estimated operators (Wiggins *et al.* 1976; Cambois & Stoffa 1992).

It should be explicitly stated that we do not impose the damped-oscillator description on the source and receiver terms. We only used this description in our synthetic experiments to obtain realistic amplitude perturbations. Therefore, this method can potentially be used to validate the damped-oscillator description for source and receiver coupling, and this could improve our understanding of source and receiver coupling effects in seismic data.

We illustrated the developed method on single component data. Application of the method to multicomponent data would in principle require repeated experiments with horizontal and vertical vibrators. Then, we have reciprocity constraints on both vertical and horizontal component recordings, and we expect results with a similar accuracy as presented in this paper for the single component case.

Interesting is whether we can still obtain corrections for the case with multicomponent recordings and a single component source. Consider multicomponent data generated by a vertical vibrator. Then, we do not have reciprocal constraints on the horizontal component recordings. Nevertheless, the following approach might be feasible. First, we can compute and apply source and receiver corrections to the vertical component data using the method presented in this paper. Then, it might be possible to derive corrections for the horizontal component data using the proposed regularization criteria, that is, using the energy constraints and the minimum variation constraints.

Finally, we only considered the decomposition of amplitudes into source, receiver, and medium response terms in the log/Fourier domain. Problems associated to the phase are due to the cycle skips of the phase: only the principal value of the original phase is known, and this introduces discontinuities in the phase function. We did not succeed in finding a suitable regularization for the inverse problem to perform the decomposition of the phase in source, receiver, and medium response terms. Thus, finding a pre-processing method to compensate data for source and receiver phase perturbations is subject of future research. Nevertheless, phase perturbations can be dealt with during the later stages of the processing, for example, residual static corrections. It should be noted that the performance of cross-correlation based methods, which are commonly used for estimating time differences, is better after waveform equalization, which is achieved with the presented method.

8 CONCLUDING REMARKS

Existing surface-consistent deconvolution techniques are applicable to primary reflection data only, and assume that common-depth point gathering is valid. Since multichannel filter operations, which are commonly used to suppress ground roll and multiples, are sensitive to source and receiver perturbations, corrections for these effects should be done in the early stages of the processing sequence.

We presented a pre-processing technique to compensate for these source and receiver perturbations, which is applicable to the whole seismic trace. Furthermore, it does not impose additional requirements on the subsurface. The approach is based on reciprocity of the medium response, so that differences between normal and reciprocal recordings can be attributed to the source and receiver perturbations.

Reciprocity does not fully constrain lateral source and receiver amplitude perturbations. Additional information is required to obtain a unique solution to the inverse problem. We used a criterion based on minimizing energy total differences between adjacent common source and receiver gathers, and based on minimizing variation in common-offset panels of the medium response.

We developed the theoretical framework both for single and multicomponent data. Synthetic tests on single component data demonstrated that this method significantly reduces the effects of lateral source and receiver variations.

ACKNOWLEDGMENTS

The authors would like to thank Kees Wapenaar and an anonymous reviewer for their constructive comments. Furthermore, we acknowledge Schlumberger for financially supporting this research project.

REFERENCES

- Alford, R.M., 1986. Shear data in the presence of azimuthal anisotropy: Dilley, Texas, in *Soc. Expl. Geophys., Expanded Abstracts*, pp. 476–479.
- Auld, B.A., 1973. *Acoustic fields and waves in solids: Vol. 1*, John Wiley & Sons, Inc., New York, NY.
- Cambois, G. & Stoffa, P.L., 1992. Surface-consistent deconvolution in the log/Fourier domain, *Geophysics*, **57**, 823–840.
- Cary, P.W. & Lorentz, G.A., 1993. Four-component surface-consistent deconvolution, *Geophysics*, **58**, 383–392.

- Castagna, J.P. & Backus, M.M., 1993. *Offset-dependent reflectivity—Theory and practice of AVO analysis*, Soc. Expl. Geophys., Tulsa, OK.
- Deal, M.M. & Nolet, G., 1996. Nullspace shuttles, *Geophys. J. Int.*, **124**, 372–380.
- Drijkoningen, G.G., 2000. On the usefulness of ground-coupling experiments to seismic data, *Geophysics*, **65**, 1780–1787.
- Fenati, D. & Rocca, F., 1984. Seismic reciprocity field tests from the Italian Peninsula, *Geophysics*, **49**, 1690–1700.
- Hoover, G.M. & O'Brien, J.T., 1980. The influence of the planted geophone on seismic land data, *Geophysics*, **45**, 1239–1253.
- Karrenbach, M., 1994. Multicomponent source equalization, in *Soc. Expl. Geophys., Expanded Abstracts*, pp. 1449–1452.
- Kelamis, P.G. & Verschuur, D.J., 2000. Surface-related multiple elimination on land seismic data—Strategies via case studies, *Geophysics*, **65**, 719–734.
- Knopoff, L. & Gangi, A.F., 1959. Seismic reciprocity, *Geophysics*, **24**, 681–691.
- Krohn, C., 1984. Geophone ground coupling, *Geophysics*, **49**, 722–731.
- Lanczos, C., 1961. *Linear Differential Operators*, Van Nostrand, London.
- Levin, S.A., 1989. Surface-consistent deconvolution, *Geophysics*, **54**, 1123–1133.
- Li, X. & MacBeth, C., 1997. Data-matrix asymmetry and polarization changes from multicomponent surface seismics, *Geophysics*, **62**, 630–643.
- Luo, H. & Li, Y., 1998. The application of blind channel identification techniques to prestack seismic deconvolution, *Proc. IEEE*, **86**, 2082–2089.
- Menke, W., 1984. *Geophysical data analysis: discrete inverse theory*, Academic Press, New York, NY.
- Michaud, G. & Snieder, R., 2004. Error in shear-wave polarization and time splitting, *Geophys. Prospect.*, **52**, 123–132.
- Newman, P. & Mahoney, J.T., 1973. Patterns—with a pinch of salt, *Geophys. Prospect.*, **21**, 197–219.
- Ostrander, W.J., 1984. Plane-wave reflection coefficients for gas sands at nonnormal angles of incidence, *Geophysics*, **49**, 1637–1648.
- Robertsson, J.O.A., Blanch, J.O. & Symes, W.W., 1994. Viscoelastic finite-difference modeling, *Geophysics*, **59**, 1444–1456.
- Sallas, J.J., 1984. Seismic vibrator control and the downgoing *P*-wave, *Geophysics*, **49**, 732–740.
- Taner, M.T. & Koehler, F., 1981. Surface consistent corrections, *Geophysics*, **46**, 17–22.
- Tarantola, A., 1987. *Inverse problem theory*, Elsevier, Amsterdam.
- Tatham, R.H. & McCormack, M.D., 1991. *Multicomponent seismology in petroleum exploration*, Soc. Expl. Geophys., Tulsa, OK.
- Van Vossen, R., Curtis, A., Laake, A. & Trampert, J., 2005. Surface-consistent deconvolution using reciprocity and waveform inversion, *Geophysics*, **71**, V19–V30.
- Wapenaar, C.P.A., Herrmann, P., Verschuur, D.J. & Berkhout, A.J., 1990. Decomposition of multicomponent seismic data into primary *P*- and *S*-wave responses, *Geophys. Prospect.*, **38**, 633–661.

- White, J.E., 1960. Use of reciprocity theorem for computation of low frequency radiation patterns, *Geophysics*, **25**, 613–624.
- Wiggins, R.A., Lerner, K.L. & Wisecup, R.D., 1976. Residual static analysis as a general linear inverse problem, *Geophysics*, **41**, 922–938.

APPENDIX A: STRUCTURE OF THE COEFFICIENT MATRIX **A**

In this section, we illustrate the structure of the data vector $\mathbf{d}(\omega)$, the model vector $\mathbf{m}(\omega)$, and the coefficient matrix **A** for single component data. We adopted the matrix-vector notation

$$\mathbf{d}(\omega) = \mathbf{A}\mathbf{m}(\omega), \quad (\text{A1})$$

to analyse the constraints on $\mathbf{m}(\omega)$ given by the convolutional model and reciprocity. Here, we give the expressions for $\mathbf{d}(\omega)$, $\mathbf{m}(\omega)$, and **A** for a configuration with two coincident source and receiver positions. It is straightforward to generalize the obtained expressions for *N* coincident source–receiver positions and for multicomponent ($3C \times 3C$) recordings.

We denote the data generated by the *i*th source and the *j*th receiver with V_{ij} , the source term of the *i*th source with S_i , and the receiver term of the *j*th receiver with R_j . Then, the data vector **d** can be written as:

$$\mathbf{d} = (V_{11} \ V_{12} \ V_{21} \ V_{22})^T. \quad (\text{A2})$$

We order the unknown terms in the model vector according to:

$$\mathbf{m} = (G_{11} \ G_{12} \ G_{22} | R_1 \ R_2 | S_1 \ S_2)^T. \quad (\text{A3})$$

Note that reciprocity is used to reduce the number of unknown Green's functions explicitly: G_{ij} not only denotes the Green's function for data generated by the *i*th source and the *j*th receiver, but also for the reversed source–receiver positions. Given the data and model vectors, the coefficient matrix reads:

$$\mathbf{A} = \left(\begin{array}{ccc|cc|cc} 1 & 0 & 0 & 1 & 0 & 1 & 0 \\ 0 & 1 & 0 & 0 & 1 & 1 & 0 \\ 0 & 1 & 0 & 1 & 0 & 0 & 1 \\ 0 & 0 & 1 & 0 & 1 & 0 & 1 \end{array} \right). \quad (\text{A4})$$

The vertical lines in this matrix indicate the separation between the columns corresponding to the medium response terms, receiver terms, and source terms, respectively. The entries in **A** relate the data vector components to the unknown model components: they describe the decomposition of the data according to the convolutional model in the log/Fourier domain (eq. 6).